iScience

CellPress
OPEN ACCESS

Article

Intracellular magnetic hyperthermia reverses sorafenib resistance in hepatocellular carcinoma through its action on signaling pathways

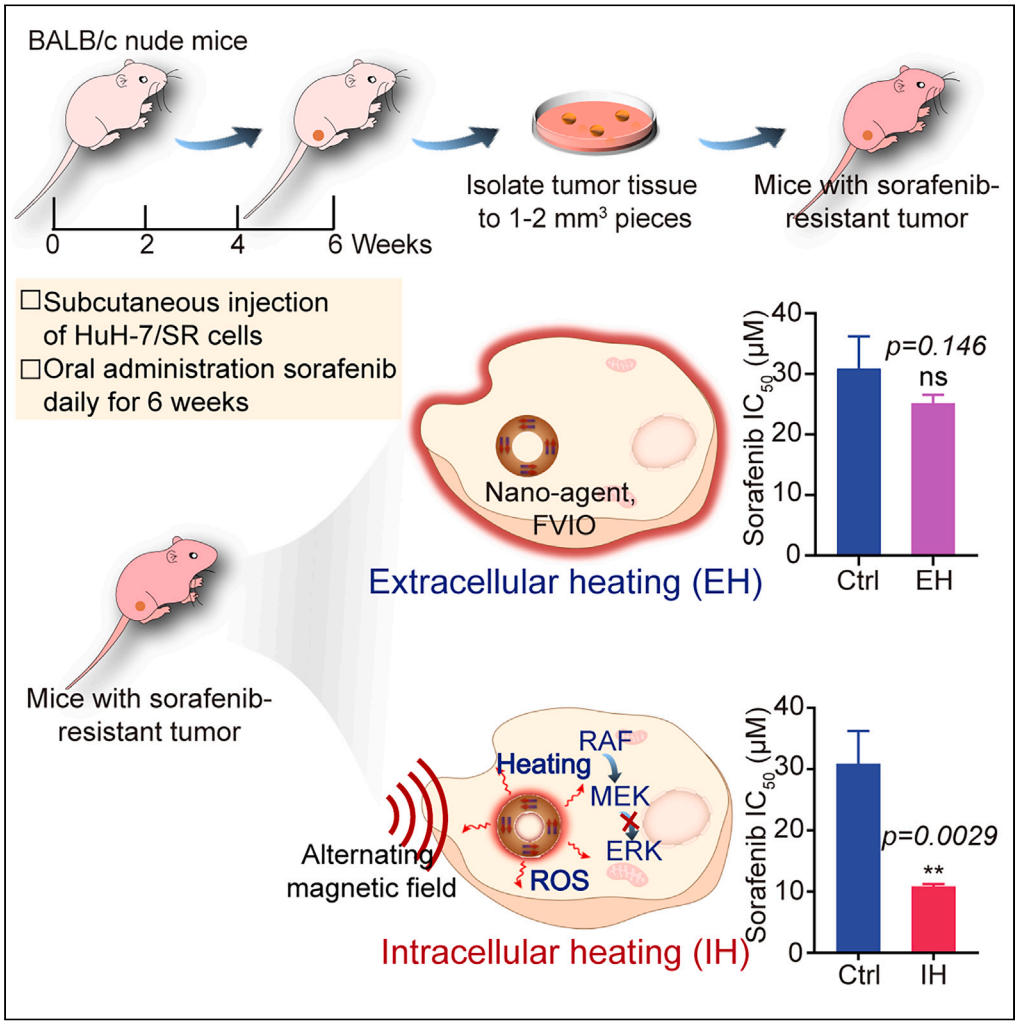

Hugang Li, Zirui Ye, Xun Wang, ..., Haiming Fan, Yi Lyu, Xiaoli Liu

yanbin@xjtu.edu.cn (B.Y.)
luyi169@126.com (Y.L.)
liuxiaoli0108@xjtu.edu.cn (X.L.)

Highlights

Intracellular MH overcomes sorafenib resistance, unlike exogenous hyperthermia

Intracellular MH reverses sorafenib resistance via ROS-MEK-ERK pathway downregulation

MH enhances tumor sensitivity to sorafenib, suppressing growth and improving survival

Li et al., iScience 27, 110029
June 21, 2024
https://doi.org/10.1016/j.isci.2024.110029

iScience

CellPress
OPEN ACCESS

Article

Intracellular magnetic hyperthermia reverses sorafenib resistance in hepatocellular carcinoma through its action on signaling pathways

Hugang Li,[1,3] Zirui Ye,[1,2] Xun Wang,[4] Jianlan Yuan,[4] Jingyi Guo,[4] Chen Liu,[4] Bin Yan,[1,2,*] Haiming Fan,[4,5] Yi Lyu,[1,2,3,*] and Xiaoli Liu[1,2,3,4,6,*]

SUMMARY

Sorafenib, a first-line drug for advanced hepatocellular carcinoma (HCC), unfortunately encounters resistance in most patients, leading to disease progression. Traditional approaches to counteract this resistance, particularly those targeting the RAF-MEK-ERK pathway, often face clinical feasibility limitations. Magnetic hyperthermia (MH), unlike conventional thermal therapies, emerges as a promising alternative. It uniquely combines magnetothermal effects with an increase in reactive oxygen species (ROS). This study found the potential of intracellular MH enhanced the efficacy of sorafenib, increased cellular sensitivity to sorafenib, and reversed sorafenib resistance by inhibiting the RAF-MEK-ERK pathway in an ROS-dependent manner in a sorafenib-resistant HCC cell. Further, in a sorafenib-resistant HCC mouse model, MH significantly sensitized tumors to sorafenib therapy, resulting in inhibited tumor growth and improved survival rates. This presents a promising strategy to overcome sorafenib resistance in HCC, potentially enhancing therapeutic outcomes for patients with this challenging condition.

INTRODUCTION

Liver cancer, with hepatocellular carcinoma (HCC) as the major subtype, is a significant global health concern, ranking as the most common malignancy worldwide and fourth leading cause of cancer-related death.[1–3] HCC is often diagnosed at an intermediate or advanced stage, at which point systemic anti-cancer therapy becomes the primary treatment option.[2,4,5] Sorafenib, a multi-targeted kinase inhibitor was approved by the US Food and Drug Administration in 2008, is a first-line treatment for advanced HCC. It targets several kinases, including rapidly accelerated fibrosarcoma (RAF) kinase, vascular endothelial growth factor receptors (VEGFRs), platelet-derived growth factor receptors, KIT proto-oncogene receptor tyrosine kinase, and FMS-related tyrosine kinase 3.[4,6] Sorafenib's action mechanism involves inhibiting tumor cell proliferation by affecting the mitogen-activated protein kinase (RAF-MEK-ERK) pathway to directly suppress tumor growth and influences the VEGF-VEGFR pathway to indirectly suppress tumor angiogenesis.[3]

Despite its initial efficacy, the effectiveness of sorafenib is significantly compromised due to the rapid development of drug resistance, often occurring within several months of treatment commencement.[3,7–9] This resistance severely limits the long-term effectiveness of sorafenib in treating advanced HCC. Regorafenib, the second-line treatment option, also failed to adequately address sorafenib resistance.[10] The root cause of this resistance is often linked to the abnormal expression and interaction of intracellular signaling pathway targets, particularly the RAF-MEK-ERK signaling pathway. This pathway, vital for stress response,[11] becomes overactivated in drug-resistant tumor cells, leading to increased tumor cell proliferation, reduced apoptosis, and enhanced angiogenesis.[12–15] Despite some reports of MEK-ERK inhibitors reversing sorafenib-induced resistance,[16,17] their clinical application remains limited due to issues such as inhibitors resistance, poor *in vivo* stability, and high toxicity.[16–19]

In this context, our study explores the potential of intracellular magnetic hyperthermia (MH) therapy, as a novel approach of counteract sorafenib resistance in HCC. MH therapy, a variation of thermotherapy, can selectively eradicate cancer cells while preserving adjacent healthy tissues.[20–24] It achieves this through nanoscale thermal effects and amplified reactive oxygen species (ROS) levels at the subcellular level, unlike conventional thermal therapies which are limited to broader tissue-level effects. These properties of MH therapy are conducive to

[1]National Local Joint Engineering Research Center for Precision Surgery & Regenerative Medicine; Shaanxi Province Center for Regenerative Medicine and Surgery Engineering Research; Shaanxi Provincial Key Laboratory of Magnetic Medicine; First Affiliated Hospital of Xi'an Jiaotong University, Xi'an, Shaanxi 710061, China
[2]Institute of Regenerative and Reconstructive Medicine, Med-X Institute, First Affiliated Hospital of Xi'an Jiaotong University, Xi'an, Shaanxi 710049, China
[3]School of Future Technology, Xi'an Jiaotong University, Xi'an, Shaanxi 710049, China
[4]Laboratory of Resource Biology and Biotechnology in Western China, Ministry of Education; Provincial Key Laboratory of Biotechnology of Shaanxi Province, Northwest University, Xi'an, Shaanxi 710069, China
[5]Key Laboratory of Synthetic and Natural Functional Molecule of the Ministry of Education, College of Chemistry and Materials Science, Northwest University, Xi'an 710127, China
[6]Lead contact
*Correspondence: yanbin@xjtu.edu.cn (B.Y.), luyi169@126.com (Y.L.), liuxiaoli0108@xjtu.edu.cn (X.L.)
https://doi.org/10.1016/j.isci.2024.110029

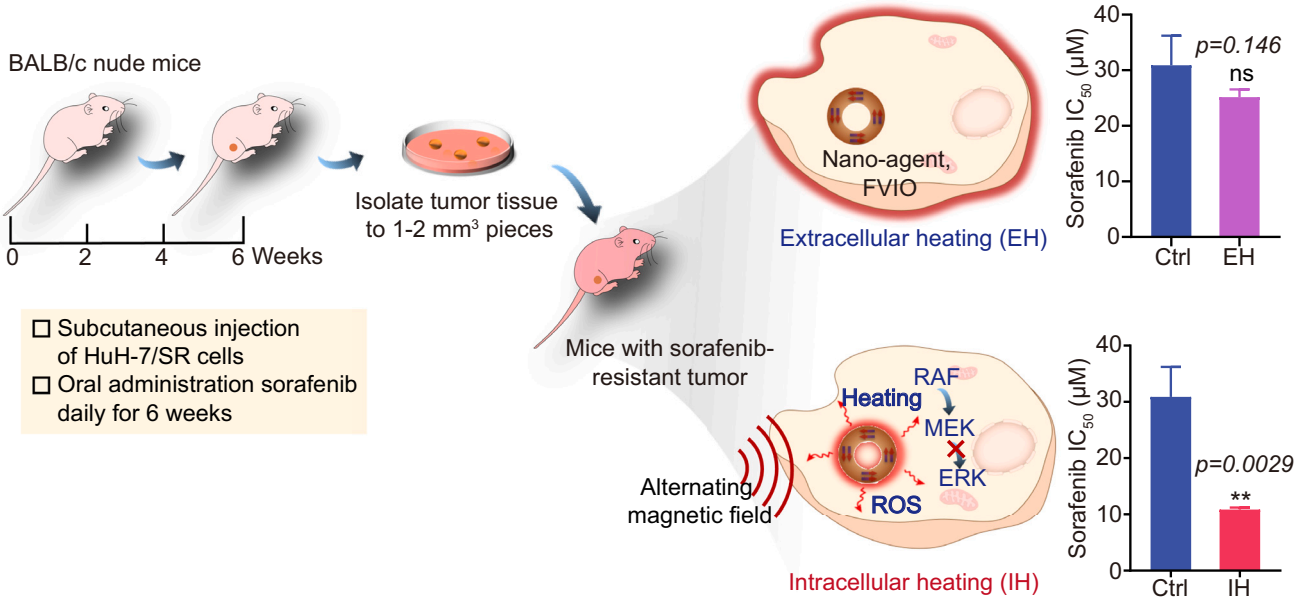

Figure 1. Illustration of FVIO-mediated intracellular MH reversing sorafenib resistance in HCC rather than extracellular heating

triggering intracellular stress responses and regulating various intracellular signaling pathways,[25–27] potentially reversing sorafenib resistance. Our research shows that using ferrimagnetic vortex-domain iron oxide nanoring (FVIO) with high magnetothermal conversion efficiency in MH therapy can effectively reverse sorafenib resistance in HCC models. In sorafenib-resistant HuH-7/SR cells, FVIO-mediated MH not only reversed resistance but also did so independent of its cytotoxic effects, indicated by similar half-maximal inhibitory concentration (IC_{50}) values to non-resistant cells. Mechanistic studies showed that FVIO-mediated MH downregulates phosphorylated ERK protein in the RAF-MEK-ERK axis via ROS-dependent mechanisms. Notably, similar effects were not replicated with exogenous hyperthermia under comparable conditions (Figure 1). This approach sensitized sorafenib-resistant tumors to therapy in a xenograft mouse model, suggesting MH therapy as a promising strategy to overcome drug resistance in HCC.

RESULTS AND DISCUSSION

FVIO-mediated MH reverses sorafenib resistance in HCC cells

FVIO was synthesized using previously reported methods.[20,23,24,28–31] The as-synthesized FVIO displayed a ring morphology with an average outer diameter of about 61 nm (Figures 2A and 2B), which aligns with the intended structural design of the nanoring. X-ray diffraction analysis revealed an inverse spinel crystal structure, typical of cubic spinel Fe_3O_4. The characteristic diffraction peaks were successfully indexed to the (220), (311), (400), (422), (511), and (440) planes of cubic spinel Fe_3O_4, as depicted in Figure 2C. To enhance hydrophilicity, dopamine was bound to the surface of FVIO, forming FVIO colloids (FVIO-Dopa) (Figure 2D). Dynamic light scattering analyses showed that the hydrodynamic size of hydrophilic FVIO was approximately 74.02 $\pm$ 10.79 nm in an aqueous solution (Figure 2E). During the 1-week observation, the hydrodynamic diameter of FVIO remained consistent in both deionized water and DMEM culture medium, demonstrating its stability in these environments (Figure S1A). Additionally, the hydrophilic FVIO exhibited a positive zeta potential of +32.23 mV (Figure S1B), suggesting good colloidal stability. Crucially, the magnetothermal conversion efficiency, a critical parameter for evaluating its efficacy in MH, was determined. The specific absorption rate (SAR) value, a quantitative measure of this efficiency, was calculated from the temperature increase over time under an alternating magnetic field (AMF) with a frequency (f) of 365 kHz and a field strength (H) of 300 Oe. Specifically, the equation ($SAR = C\frac{\Delta T}{\Delta t}\frac{1}{m_{Fe}}$) was used to calculate SAR value, where $\Delta T/\Delta t$ is the initial slope, C is the specific heat capacity of the water, and m_{Fe} is the mass concentration of Fe in the samples. We examined the time-dependent heating profiles of FVIO at different Fe concentrations (50, 100, and 150 μg/mL) under an AMF. We calculated the SAR values and observed that SAR values across different FVIO concentrations did not show significantly changes (Figures S2A and S2B). The SAR value of hydrophilic FVIO was found to be 2,107 $\pm$ 156 W/g (Figure 2F), indicating a high efficiency of magnetothermal conversion, which is vital for the effective application of MH in biomedical contexts.

We established a sorafenib-resistant HCC cell line, HuH-7/SR, by prolonged exposure to incrementally increasing concentration of sorafenib, as illustrated in Figure 3A. The degree of resistance developed by these cells was quantified by comparing their IC_{50} values for sorafenib to those of the parental HuH-7 cells. The IC_{50} value for the HuH-7/SR cells was significantly higher at 36.14 μM compared to 12.93 μM in the parental HuH-7 cells (Figure 3B), indicating a marked decrease in sorafenib's potency against the resistant cell line.

Furthermore, we evaluated the cytotoxicity of FVIO-mediated MH in both HuH-7/SR and HuH-7 cells using a cell counting kit-8 (CCK-8) assay. This assay revealed that cell viability remained relatively high (above 80%) for both cell lines at FVIO concentrations up to 75 μg/mL

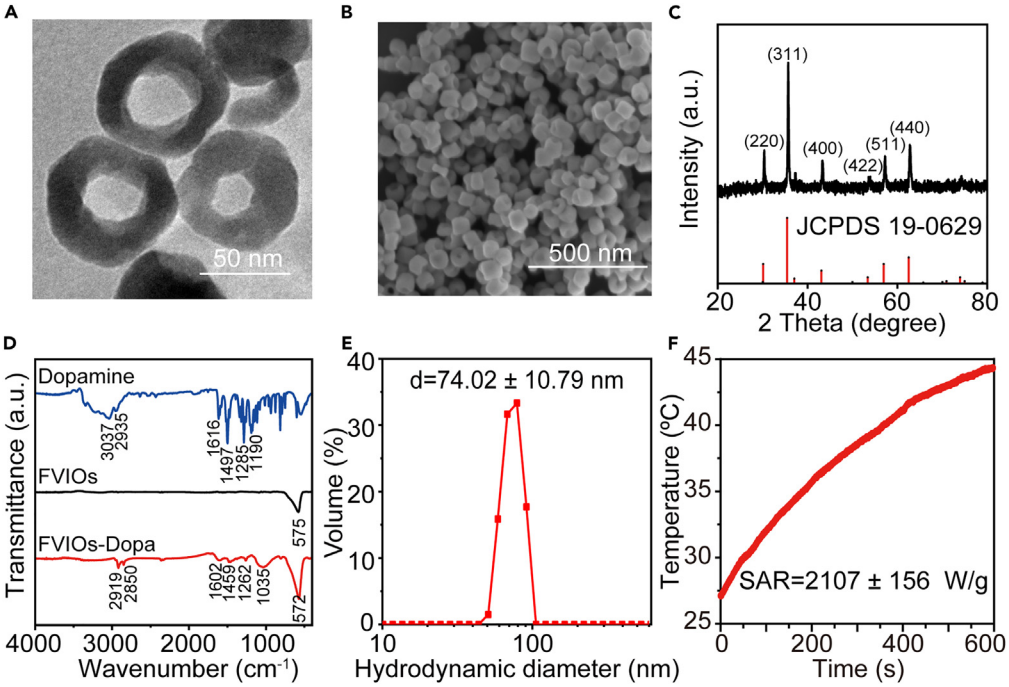

Figure 2. Characterization of FVIO

(A) Transmission electron microscope (TEM) image of FVIO. Scale bar: 50 nm.

(B) Scanning electron microscope (SEM) image of FVIO. Scale bar: 500 nm.

(C) X-ray diffraction patterns of FVIO.

(D) Fourier transform infrared spectroscopy spectra of dopamine-modified FVIO (FVIO-Dopa), FVIO, and dopamine.

(E) Hydrodynamic diameters of FVIO.

(F) Time-dependent heating profiles of 1 mL of FVIO (100 μg/mL) suspension under alternating magnetic field (AMF) (360 kHz, 300 Oe).

Fe, suggesting that the hydrophilic FVIO alone exhibited minimal cytotoxicity (Figures S3A and S3B). However, upon treatment with FVIO-mediated MH, a notable decrease in cell viability was observed in both HuH-7/SR and HuH-7 cells, showing a dependence on the concentration of Fe used. Specifically, after exposure to an AMF at a frequency of 365 kHz and a field strength of 300 Oe for 10 min, the viability of cells incubated with 75 μg/mL Fe of FVIO dropped to approximately 56.8% for HuH-7/SR cells and 55.3% for HuH-7 cells (Figures S3C and S3D). This reduction in cell viability was even more pronounced at a higher Fe concentration of 100 μg/mL, decreasing to around 35.8% in HuH-7/SR cells and 37.0% in HuH-7 cells. Following co-incubating 75 μg/mL FVIO with HuH-7/SR cells, the intracellular Fe ion concentration was detected using an inductively coupled plasma mass spectrometer. The result showed that the maximum accumulation (50.76 pg/cell) of FVIO occurred at a time of 24 h (Figure S4), and the cellular uptake of FVIO showed almost no change when the co-incubation times were prolonged.

To assess the effectiveness of FVIO-mediated MH in reversing sorafenib resistance, we conducted a detailed study on HuH-7/SR cells, specifically focusing on those that survived the MH treatment. Initially, cells undergoing apoptosis as a result of MH treatment were identified and excluded from further analysis, as shown in Figure 3C. According to the CCK-8 assay results, the cell viabilities of the left HuH-7/SR cells approximately were 100% and 96%, when treated with 50 μg/mL and 75 μg/mL Fe of FVIO-mediated MH, respectively (groups 4 and 7 in Figure 3D). The high survival rate of these cells post-MH treatment allowed us to concentrate on the surviving cell population, providing a valuable opportunity to further explore how FVIO-mediated MH influences sorafenib resistance in these cells. We then proceeded to examine the functionality and cellular architecture of the remaining HuH-7/SR cells post-MH treatment (Figure 3C). We noted significant cytotoxic effects when sorafenib was combined with FVIO-mediated MH in treating HuH-7/SR cells, as shown in groups 5 and 8 of Figure 3D. Interestingly, this enhanced cytotoxicity was not observed in groups treated with FVIO alone followed by sorafenib (groups 3 and 6 in Figure 3D). While sorafenib combined with 50 μg/mL Fe FVIO-mediated MH (group 5 in Figure 3D) showed a certain level of cytotoxicity, this effect was markedly enhanced when the FVIO concentration was increased to 75 μg/mL Fe (group 8 in Figure 3D). Remarkably, FVIO-mediated MH at 50 μg/mL Fe reduced the IC_{50} value of sorafenib from 30.69 to 22.10 μM, and at 75 μg/mL Fe, it further reduced this value to 10.84 μM (Figure 3E; Figure S5). This observation suggests that the combination of MH and sorafenib effectively mitigates resistance in sorafenib-resistant HuH-7/SR cells, with a more pronounced reduction at the higher concentration of FVIO. Control experiments, involving either FVIO plus sorafenib or AMF plus sorafenib without the MH treatment, did not exhibit a similar reduction in the IC_{50} value (Figure 3E; Figure S5).

To determine the impact of the duration of MH on the efficacy of sorafenib, we further detected the IC_{50} values of sorafenib in HuH-7/SR cells treated with different durations of FVIO-mediated MH. Following the removal of apoptotic cells post-MH treatment, CCK-8 analysis showed

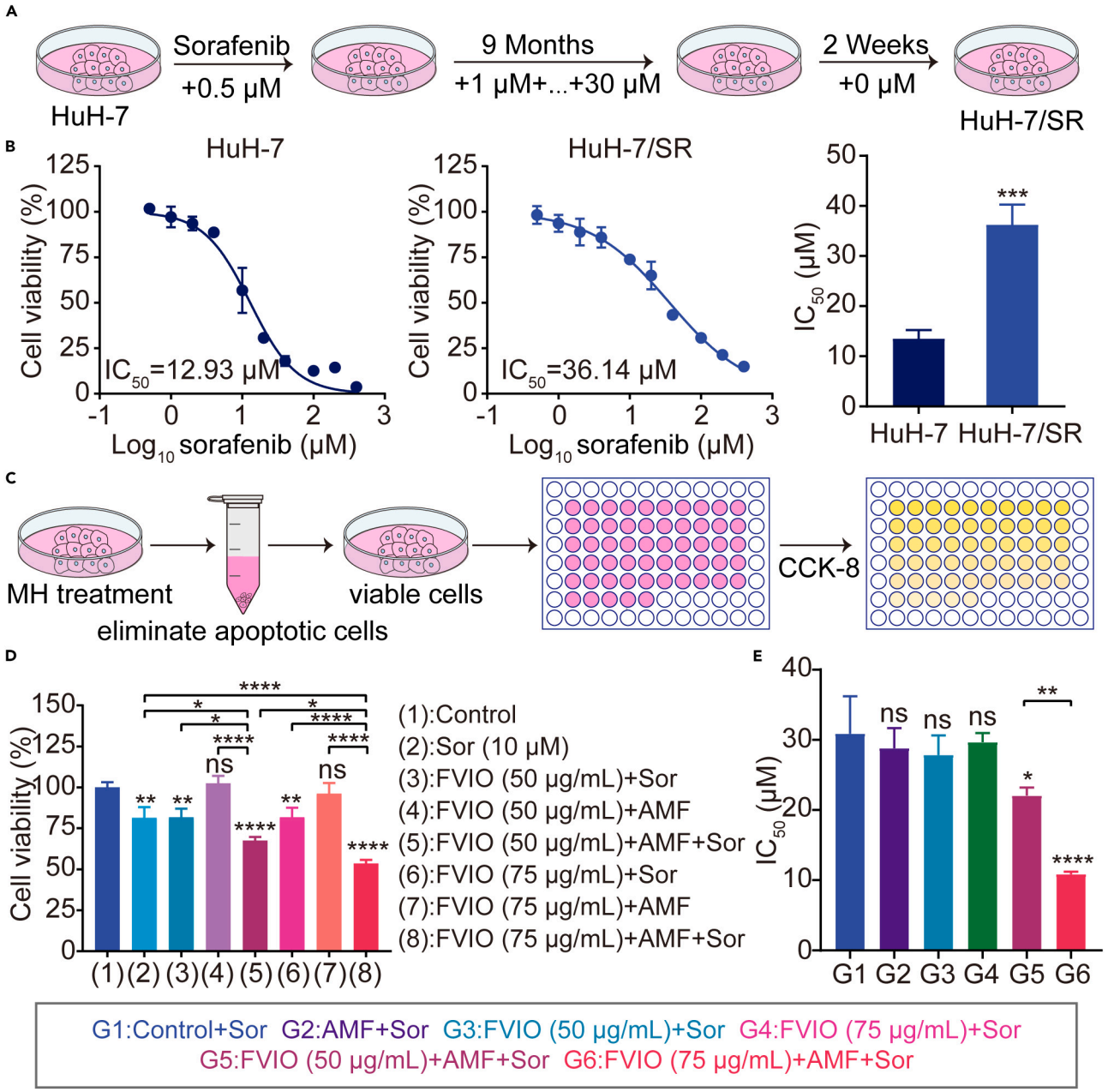

Figure 3. FVIO-mediated MH reverses sorafenib resistance in HCC cells

(A) A schematic diagram of the construction of sorafenib-resistant cells. Sorafenib-resistant HuH-7/SR cells were exposed to increasing concentrations (0.5, 1, 2, 5, 10, 15, 20, 25, and 30 μM) for 2 weeks at each concentration.

(B) The IC_{50} values of HuH-7 and HuH-7/SR cells were determined by incubating cells with increasing concentrations of sorafenib (0, 0.5, 1, 2, 4, 10, 20, 40, 100, 200, and 400 μM).

(C) The experimental process used to determine the IC_{50} values of sorafenib after HuH-7/SR cells were treated with FVIO-mediated MH.

(D) The cell viability of HuH-7/SR cells after treatment with DMEM, sorafenib (Sor: 10 μM, incubation 48 h), FVIO (50 or 75 μg/mL, incubation 24 h) plus sorafenib, FVIO-mediated MH (FVIO: 50 or 75 μg/mL, incubation 24 h; AMF: 300 Oe, 10 min), and MH plus sorafenib.

(E) The IC_{50} values of sorafenib in HuH-7/SR cells treated with DMEM, AMF (300 Oe, 10 min), FVIO (50 or 75 μg/mL, incubation 24 h), or MH (FVIO: 50 or 75 μg/mL, incubation 24 h; AMF: 300 Oe, 10 min). Values are the means ± SD from three independent experiments. Statistical differences were determined by the Student's t test and one-way ANOVA with Tukey's multiple comparison tests. The range of p values is indicated by the number of asterisks *$p < 0.05$, **$p < 0.01$, ***$p < 0.001$, ****$p < 0.0001$; ns, no significance $p > 0.05$.

that the cell viabilities of the HuH-7/SR cells were 86.87%, 96.10%, and 85.37%, when the durations of FVIO-mediated MH were 5, 10, and 15 min, respectively (group 3, 5, and 7 in Figure S6A). Interestingly, FVIO-mediated MH for the duration of 5 min in combination with sorafenib showed significant cytotoxicity, which remained unchanged when the duration was extended to 15 min (group 2, 4, 6, and 8 in Figure S6A). In addition, FVIO-mediated MH for the duration of 5 min reduced the IC_{50} value of sorafenib in HuH-7/SR cells from 31.17 to 19.39 μM. Extending the duration to 10 and 15 min decreased the IC_{50} values to 10.84 and 10.72 μM, respectively (detailed in Figures S6B and S6C). This result showed that there was no significant difference between the duration of 10 and 15 min for FVIO-mediated MH action on reversal of sorafenib resistance. To minimize the impact of FVIO-mediated MH on cell viability, the duration of 10 min was chosen to investigate the potential mechanisms of FVIO-mediated MH on reversal of sorafenib resistance in HuH-7/SR cells. These finding underscores the unique contribution of MH in enhancing the sensitivity of HuH-7/SR cells to sorafenib. These results collectively indicate that FVIO-mediated MH is an effective strategy for sensitizing sorafenib-resistant HCC cells to treatment, independent of the direct cytotoxic effects of the FVIO-mediated MH.

Mechanism of sorafenib resistance and impact of FVIO-mediated MH on the MEK-ERK axis

Previous studies have identified the overactivation of the RAF-MEK-ERK signaling pathway as a key factor in the development of sorafenib resistance in HCC cells, including resistance to inhibitors targeting RAS, RAF, and MEK.[16,17,32] In this current work, western blot analysis revealed elevated levels of phosphorylated MEK (p-MEK) and ERK (p-ERK) in sorafenib-resistant HuH-7/SR cells compared to HuH-7 cells (Figures S7A and S7B), corroborating these findings. This overactivation suggests a critical role of the MEK-ERK axis in sorafenib resistance. Our hypothesis was that FVIO-mediated MH could potentially reverse this resistance by modulating the MEK-ERK pathway.

Previous reports indicate that FVIO-mediated MH generates nanoscale magnetothermal heating and intracellular ROS in various cancer cell lines.[29,30] In this study, treatment with FVIO-mediated MH (75 μg/mL Fe) significantly increased both temperature and intracellular ROS production in HuH-7/SR cells, as illustrated in Figures 4A and 4B. Since ERK is a downstream transducer in ROS-mediated signaling,[33–36] we observed a decrease in p-ERK expression following treatment with FVIO-mediated MH (75 μg/mL Fe) in HuH-7/SR cells. This decrease was reversed upon the introduction of ROS scavenger N-acetylcysteine (3 mM; Figures 4C–4E). Intriguingly, when we replicated the conditions of FVIO-mediated MH using exogenous hyperthermia (EH) via water bath heating (maintaining the same Fe concentration of 75 μg/mL and treatment duration of 10 min), we did not observe a reduction in p-ERK levels in the HuH-7/SR cells. After EH treatment of HuH-7/SR cells, we did not observe a significant difference in the IC_{50} value compared to the control (Figures S8A and S8B).

We further examined the protein expression of the MEK-ERK pathway in HuH-7/SR cells after FVIO-mediated MH treatment at varying Fe concentrations (ranging from 0 to 75 μg/mL). A distinct Fe concentration-dependent effect was observed, where higher concentrations of Fe in the MH treatment corresponded to more pronounced downregulation of p-ERK (Figures 4F–4H). This finding is crucial as it demonstrates a dose-dependent efficacy of MH in modulating key signaling pathways in HCC cells. This outcome, detailed in Figure 4, is particularly significant as it highlights the specificity of the MH-induced effects. It underscores that the observed downregulation of p-ERK is not merely a consequence of increased temperature but is instead attributed to the unique ROS-dependent mechanism triggered by FVIO-mediated MH. This distinction is critical for understanding the therapeutic potential of MH in treating HCC, especially in the context of overcoming drug resistance.

Interestingly, our western blotting analysis indicated that p-MEK levels remained unchanged across various treatments, including control, sorafenib, and FVIO-mediated MH (with or without sorafenib) (Figures 5A and 5B). This consistency across different treatment conditions suggests that p-MEK may not be the primary target in the context of sorafenib resistance in HCC cells. Conversely, a significant variation was observed in p-ERK expression. While sorafenib alone moderately downregulated p-ERK, the combination of FVIO-mediated MH (75 μg/mL Fe) and sorafenib led to a dramatic reduction in p-ERK levels (Figures 5A and 5C). This pronounced effect implies that FVIO-mediated MH enhances the ability of sorafenib to target and degrade p-ERK, a key player in the RAF-MEK-ERK pathway.

To elucidate the specific relationship between p-ERK and sorafenib resistance induced by FVIO-mediated MH, we employed PD98059, a small-molecule inhibitor of p-ERK, and lipopolysaccharide (LPS), an agonist of p-ERK. The concentrations for these compounds (25 μM PD98059 and 2 μg/mL LPS) were selected based on cytotoxicity assay results (Figures S9A and S9B). Notably, the addition of PD98059 to the combined FVIO-mediated MH and sorafenib treatment significantly reduced p-ERK levels by 67.6%. In contrast, LPS increased p-ERK levels by 2.5 times (Figure 5C). Furthermore, PD98059 dramatically decreased the IC_{50} value of sorafenib in HuH-7/SR cells from 34.74 to 10.64 μM, whereas LPS increased it to 110 μM (Figures 5D; Figure S10). These findings collectively demonstrate that FVIO-mediated MH effectively reverses sorafenib resistance in HuH-7/SR cells, primarily by targeting and downregulating p-ERK expression in an ROS-dependent manner. The differential effects of PD98059 and LPS further underscore the pivotal role of p-ERK in mediating sorafenib resistance and its susceptibility to modulation by combined MH and sorafenib treatment.

A key aspect of our study was to determine whether FVIO-mediated MH could enhance the sensitivity of sorafenib-resistant HuH-7/SR cells to sorafenib. Our initial experiments showed that sorafenib alone had a moderate effect on the colony formation and growth of HuH-7/SR cells, reducing it to 83.7%. However, when we combined FVIO-mediated MH with sorafenib, we observed a substantial inhibition in both colony formation and cell growth, with rates plummeting to 30.6% as detailed in Figures S11A and S11B. This significant decrease highlights the potential of MH to augment the therapeutic efficacy of sorafenib. Furthermore, the combination of MH and sorafenib markedly increased the rate of apoptosis in HuH-7/SR cells. Post treatment, the apoptotic rate was 39.8%, a 2.48-fold increase compared to the sorafenib-alone group ($p = 0.0003$), as illustrated in Figures S11C and S11D. This heightened induction of apoptosis clearly demonstrates the sensitizing effect of FVIO-mediated MH on HuH-7/SR cells toward sorafenib. These findings collectively suggest that FVIO-mediated MH can significantly sensitize sorafenib-resistant HCC cells to sorafenib treatment. By markedly suppressing colony formation, inhibiting cell growth, and enhancing

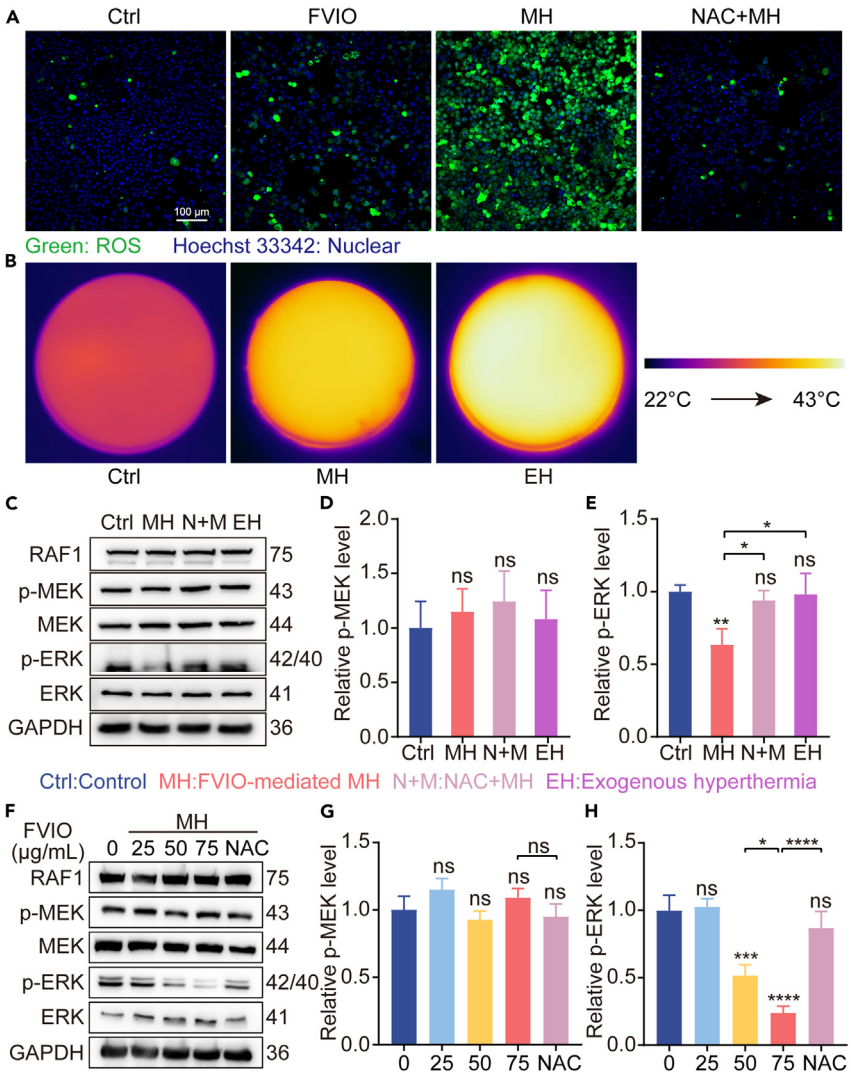

Figure 4. Mechanism of sorafenib resistance by intracellular MH

(A) Confocal laser scanning microscope (CLSM) images of HuH-7/SR cells treated after DMEM (Ctrl), FVIO (FVIO: 75 μg/mL, incubation 24 h), FVIO-mediated MH (FVIO: 75 μg/mL, incubation 24 h; AMF: 300 Oe, 10 min), or N-acetylcysteine (NAC) plus MH (N + M; NAC: 3 mM, incubation 24 h; FVIO: 75 μg/mL, incubation 24 h; AMF: 300 Oe, 10 min). ROS production was detected using DCFH-DA (green). Nuclei were stained with Hoechst 33342 (blue). Scale bar: 100 μm.

(B) Thermal images of HuH-7/SR cells treated with DMEM, MH (FVIO: 75 μg/mL, incubation 24 h; AMF: 300 Oe, 10 min), or endogenous hyperthermia (EH; FVIO: 75 μg/mL, incubation 24 h; 43°C water bath heating, 10 min) were acquired by an infrared radiation (IR) camera.

(C) The expression of proteins in the RAF-MEK-ERK pathway after HuH-7/SR cells were treated with DMEM, MH (FVIO: 75 μg/mL, incubation 24 h; AMF: 300 Oe, 10 min), NAC (3 mM, incubation 24 h) plus MH, or EH (FVIO: 75 μg/mL, incubation 24 h; 43°C water bath heating, 10 min).

(D and E) Quantitative analysis of p-MEK and p-ERK protein expression.

(F) HuH-7/SR cells were treated with FVIO-mediated MH with various Fe concentrations (0, 25, 50, and 75 μg/mL) or NAC (3 mM, incubation 24 h) plus MH (FVIO: 75 μg/mL, incubation 24 h; AMF: 300 Oe, 10 min) and the cell lysates were analyzed by western blotting.

(G and H) Quantitative analysis of p-MEK and p-ERK protein expression. Values are the means ± SD from three independent experiments. Statistical differences were determined by the Student's t test. The range of p values is indicated by the number of asterisks *$p < 0.05$, ***$p < 0.001$, ****$p < 0.0001$; ns, no significance $p > 0.05$.

apoptosis rates, MH treatment emerges as a promising strategy to improve the efficacy of sorafenib in resistant HCC cases. This synergistic interaction between MH and sorafenib offers a promising approach that could be pivotal in managing drug resistance in HCC therapy.

FVIO-mediated MH in enhancing the anti-tumor efficacy of sorafenib in a sorafenib-resistant HCC mouse model

Clinical evidence has indicated that sorafenib monotherapy, although initially effective, often results in a limited disease control rate (35.3%) in patients with advanced HCC due to the development of resistance to the drug.[8] To address this challenge and assess the potential of

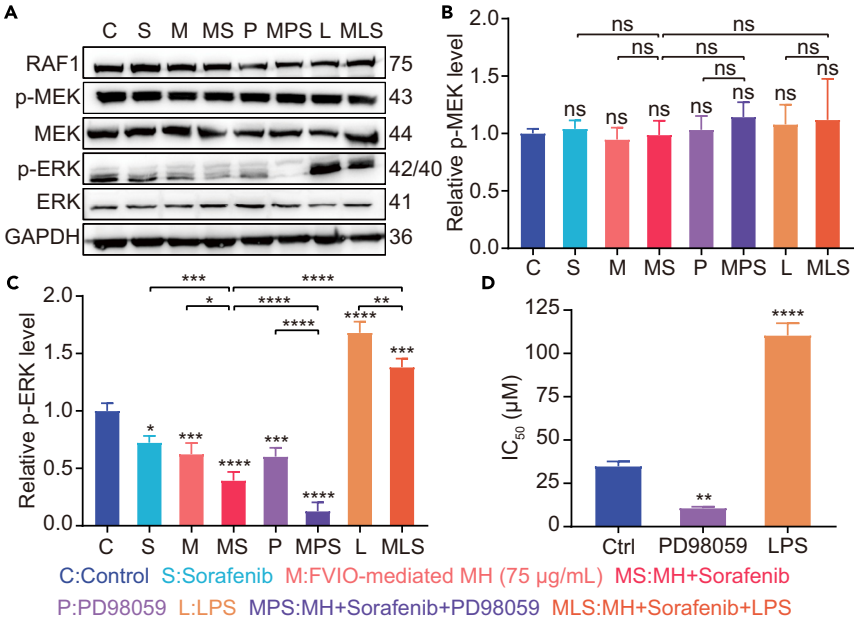

Figure 5. FVIO-mediated MH reverses sorafenib resistance in HCC cells by affecting the MEK-ERK axis

(A) Western blotting analysis of protein expression levels after HuH-7/SR cells were treated with DMEM, sorafenib (5 μM, incubation 24 h), MH (FVIO: 75 μg/mL, incubation 24 h; AMF: 300 Oe, 10 min), PD98059 (20 μM, incubation 24 h), LPS (2 μg/mL, incubation 24 h), MH plus sorafenib, MH plus PD98059 plus sorafenib, or MH plus LPS plus sorafenib.

(B and C) Quantitative analysis of p-MEK and p-ERK protein expression.

(D) The IC_{50} value of sorafenib in HuH-7/SR cells treated with DMEM, PD98059 (20 μM, incubation 24 h), or LPS (2 μg/mL, incubation 24 h), respectively. Values are means ± SD from three independent experiments. Statistical differences were determined by one-way ANOVA with Tukey's multiple comparison tests. The range of p values is indicated by the number of asterisks *$p < 0.05$, **$p < 0.01$, ***$p < 0.001$, ****$p < 0.0001$; ns, no significance $p > 0.05$.

reversing sorafenib resistance, we established a sorafenib-resistant HCC mouse model using HuH-7/SR cells. The mice were subjected to daily oral gavage with 15 mg/kg of sorafenib, as depicted in Figure 6A. After a 6-week treatment period, tumor tissues from these mice were collected and analyzed through immunohistochemical examination. Notably, we observed elevated levels of p-MEK and p-ERK in the sorafenib-treated tumors compared to non-treated controls (Figure 6B). This provided evidence of successful establishment of a sorafenib-resistant HCC mouse model, in line with previous studies.[16,37,38]

Subsequently, sorafenib-resistant tumor tissues, dissected into 1–2 mm^3 fragments, were transplanted subcutaneously into the right dorsal region of male BALB/C nude mice. Upon the tumors reaching approximately 100 mm^3, the mice were divided into six groups (5 mice per group), encompassing various treatments: (1) control, (2) sorafenib, (3) FVIO-mediated MH, (4) FVIO-mediated MH plus PD98059, (5) FVIO-mediated MH plus sorafenib, and (6) FVIO-mediated MH plus sorafenib and PD98059, as shown in Figure 6C. The treatment protocol included intra-tumoral injection of FVIO (3 mg Fe/cm^3) on day 1, followed by exposure to an AMF (300 Oe, 360 kHz) for 10 min on days 1, 3, and 5. PD98059 was administered intravenously on alternate days, and sorafenib was given daily until the end of the experiment. Infrared thermal imaging confirmed that tumor temperatures reached approximately 43°C during MH treatments (Figure S12). Throughout the 24-day study period, tumor volume and body weight were monitored every three days.

We observed distinct variations in tumor growth among different treatment groups, as shown in Figure 6D. Notably, while sorafenib alone failed to suppress tumor growth significantly, the combination of FVIO-mediated MH and sorafenib resulted in a substantial reduction of tumor growth by 71.46%. Further, the addition of PD98059 to this combination enhanced the suppression of tumor growth to 91.11%. These findings strongly suggest that FVIO-mediated MH effectively sensitizes sorafenib-resistant tumors to sorafenib therapy, leading to significant tumor growth inhibition in the HuH-7/SR tumor model. Additionally, tumor weights in the group treated with FVIO-mediated MH and sorafenib were significantly lower compared to other groups, as depicted in Figure 6E. Importantly, throughout the experimental duration, mice in the FVIO-mediated MH plus sorafenib group exhibited no notable abnormal behaviors or loss in body weight (Figure 6F). The survival analysis over 30 days, presented in Figure 6G, further underscored the effectiveness of our treatment strategies. While all mice in the control and sorafenib-only groups succumbed by day 28, those treated with FVIO-mediated MH, both with and without PD98059, showed a 20% survival rate at day 30. Remarkably, the survival rate was significantly enhanced in groups treated with the combination of FVIO-mediated MH and sorafenib, with or without PD98059. All mice in these groups survived to day 30 and exhibited significant tumor regression. Hematoxylin and eosin (H&E) staining of tumors specimens revealed that the combination treatment with FVIO-mediated MH and sorafenib resulted in chromatin condensation and disrupted tissue architecture, characteristics indicative of

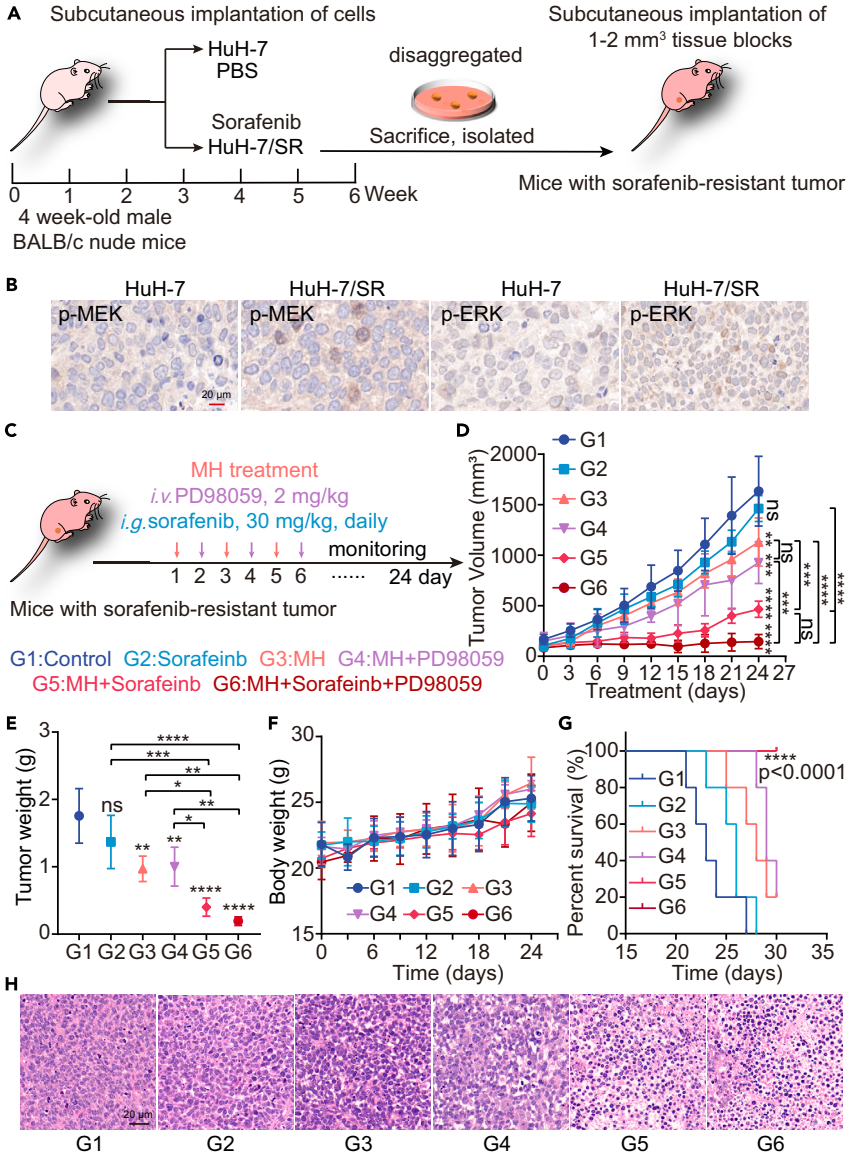

Figure 6. FVIO-mediated MH in enhancing the anti-tumor efficacy of sorafenib in a sorafenib-resistant HCC mouse model

(A) A schematic diagram showing how sorafenib-sensitive and sorafenib-resistant tumor xenografts were established.

(B) Representative images of immunohistochemical staining of tumor specimens for p-MEK and p-ERK expression in sorafenib-sensitive and sorafenib-resistant HCC models. Scale bar: 20 μm.

(C) The experimental schedule for treatment administration in the sorafenib-resistant mouse model.

(D) Tumor growth curves of different treatments in the sorafenib-resistant HCC model.

(E) The tumor weight of each treatment group of the sorafenib-resistant mouse model at the end of the experiment.

(F) The body weight of each treatment group of the sorafenib-resistant mouse model.

(G) The survival rate of the sorafenib-resistant mouse model in each treatment group.

(H) Hematoxylin and eosin (H&E) staining of tumors of each treatment group at the end of experiment. Scale bar: 20 μm. Data are expressed as the means ± SD (n = 5 mice per group). Statistical differences were determined by one-way ANOVA with Tukey's multiple comparison tests. The range of p values is indicated by the number of asterisks *p < 0.05, **p < 0.01, ***p < 0.001, ****p < 0.0001; ns, no significance p > 0.05.

necrosis in the tumor tissues (Figure 6H). These results further supported that FVIO-mediated MH enhances the sensitivity of tumors to sorafenib therapy in a sorafenib-resistant HCC model.

Immunohistochemical analysis of mouse tissue confirmed that FVIO-mediated MH downregulated p-ERK protein expression *in vivo* (Figures 7A and 7B). This observation supports our hypothesis that FVIO-mediated MH sensitizes sorafenib-resistant tumors to sorafenib therapy by targeting the MEK-ERK pathway. Histopathological examinations of vital organs, including the heart, liver, spleen, lung, kidney, and

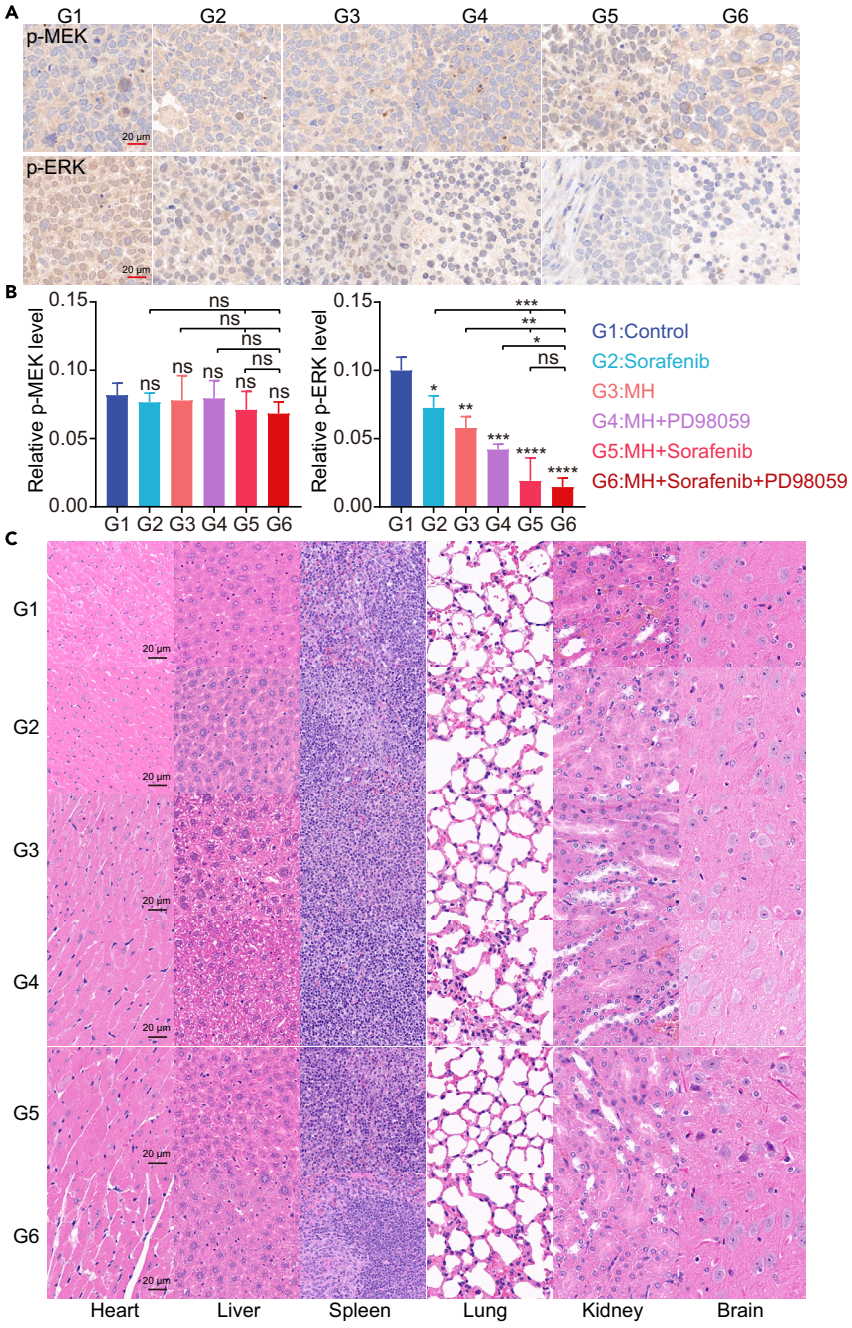

Figure 7. Histological analysis of sorafenib-resistant HCC model

(A) Representative images of immunohistochemical staining of p-MEK and p-ERK in tumor specimens from each group. Scale bar, 20 μm.

(B) The relative expression of p-MEK and p-ERK in each treatment group.

(C) H&E staining of the heart, liver, spleen, lung, kidney, and brain of the sorafenib-resistant mouse model. Scale bar, 20 μm. Data are expressed as the means ± SD. Statistical differences were determined by one-way ANOVA with Tukey's multiple comparison tests. The range of *p* values is indicated by the number of asterisks *$p < 0.05$, **$p < 0.01$, ***$p < 0.001$, ****$p < 0.0001$; ns, no significance $p > 0.05$.

brain, revealed no adverse changes (Figure 7C). In addition, we evaluated the potential cytotoxicity of FVIO in normal hepatocytes using CCK-8 assay, which indicated that the cell viability was not significantly affected after treatment with different FVIO concentrations (Figure S13). Subsequently, we investigated the *in vivo* biosafety of FVIO by injecting it into the tail veins of healthy SD rats at a dose of 5 mg/kg Fe, with saline injections serving as controls. Blood biochemistry tests were performed on days 1 and 14 after intravenous injection of FVIO. Functional indicators for the liver and kidney, including alanine aminotransferase, aspartate aminotransferase, blood urea nitrogen

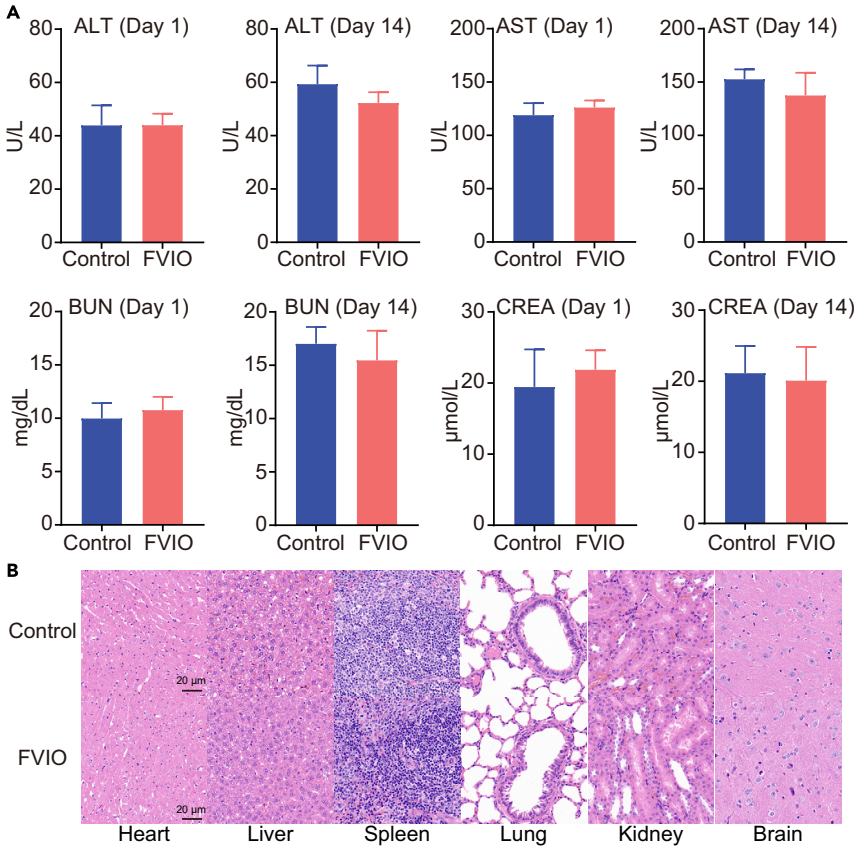

Figure 8. Biosafety of FVIO

(A) Results of blood biochemical (including ALT, AST, BUN, and CREA) in SD rats 1 day and 14 days after saline or FVIO injection.
(B) H&E staining of the heart, liver, spleen, lung, kidney, and brain of SD rats treated with saline or FVIO. Scale bar, 20 μm.

and creatinine, exhibited no significant differences between the control and FVIO groups (Figure 8A). Similarly, H&E staining of the heart, liver, spleen, lung, kidney, and brain from treated rats showed no abnormality in cellular morphology compared to those from control rats (Figure 8B). These data demonstrated the excellent biosafety of hydrophilic FVIO. In conclusion, these results collectively demonstrate the potent *in vivo* effect of FVIO-mediated MH in reversing sorafenib resistance. They offer promising insights for the development of new therapeutic strategies for HCC patients who have developed resistance to sorafenib, potentially improving outcomes in this challenging clinical scenario.

While several approaches have been explored to overcome sorafenib resistance in HCC,[39–42] they often face challenges such as low efficacy, limited targeting ability, and adverse side effects, which restrict their clinical application. Encouragingly, our study highlights the potential of FVIO-mediated MH as a promising alternative. FVIO-mediated MH effectively suppresses the activity of the MEK-ERK signaling pathway in an ROS-dependent manner, thereby facilitating the reversal of sorafenib resistance in HuH-7/SR cells. Our results indicate that FVIO-mediated MH not only decreases the IC_{50} value of sorafenib in HuH-7/SR cells but also enhances sorafenib-induced apoptosis. This dual effect suggests a heightened sensitivity of the sorafenib-resistant cells to the drug, making FVIO-mediated MH a valuable tool in combatting resistance. Furthermore, we demonstrated the efficacy of this approach *in vivo*. In a sorafenib-resistant HCC xenograft mouse model, FVIO-mediated MH significantly inhibited tumor growth, pointing to its potential in clinical settings. The findings of our study are particularly promising as they reveal a novel and effective strategy for overcoming sorafenib resistance in HCC. By targeting the MEK-ERK signaling pathway through an ROS-dependent mechanism, FVIO-mediated MH opens new avenues for enhancing the efficacy of sorafenib treatment in HCC, particularly in cases where traditional approaches have failed. This breakthrough has the potential to significantly improve therapeutic outcomes for patients suffering from this challenging form of cancer.

Conclusion

In our study, we have demonstrated that FVIO-mediated MH is capable of reversing sorafenib resistance in HCC cells resistant to this drug. A pivotal aspect of this reversal process is the modulation of the MEK-ERK signaling pathway in an ROS-dependent manner. This modulation

not only sensitizes HuH-7/SR cells to sorafenib but also significantly enhances sorafenib-induced apoptosis. It is noteworthy that this effect is attributed to the specific action of FVIO-mediated MH on signaling pathways rather than to its thermotherapeutic cytotoxicity. The implications of these findings extend beyond the scope of treating sorafenib-resistant HCC. Given the pivotal role of the MEK-ERK axis in various drug-resistant tumors, it is reasonable to speculate that FVIO-mediated MH could also enhance drug sensitivity in other types of cancer where resistance is driven by aberrant activation of this signaling axis. This possibility opens new avenues for research and potential therapeutic applications.

In conclusion, our work not only reveals a novel and effective approach to overcome sorafenib resistance in HCC but also suggests a broader potential for FVIO-mediated MH as a strategy to mitigate drug resistance in various cancers. This study contributes to the expanding field of cancer therapeutics, offering new hope for improving treatment outcomes in drug-resistant cancers.

Limitations of the study

We demonstrated that FVIO-mediated MH has the potential to reverse sorafenib resistance, which is often due to an overactive MEK-ERK pathway. Our findings indicate that MH enhances the anti-tumor efficacy of sorafenib in both HCC cells resistant to this drug and in a sorafenib-resistant HCC xenograft mouse model, primarily by inhibiting MEK-ERK pathway. However, we cannot rule out the involvement of other mechanisms in this process. Therefore, further investigation is necessary before this approach can be widely implemented in clinical practice.

STAR★METHODS

Detailed methods are provided in the online version of this paper and include the following:

- KEY RESOURCES TABLE
- RESOURCE AVAILABILITY
  - Lead contact
  - Materials availability
  - Data and code availability
- EXPERIMENTAL MODEL AND STUDY PARTICIPANT DETAILS
- METHOD DETAILS
  - Preparation of FVIO
  - Characterization of FVIO
  - Measurement of SAR value
  - Induction of a sorafenib-resistant cell line
  - Half maximal inhibitory concentration assay
  - MH treatment and water bath heating of HuH-7/SR cells
  - Cellular uptake assay
  - *In vitro* cell cytotoxicity
  - Colony formation assay and cell growth curve
  - Cell apoptosis assay
  - Analysis of *in vitro* ROS generation
  - Western blotting assay
  - Development of a sorafenib-resistant HCC mouse model
  - Immunohistochemistry analysis and hematoxylin-eosin staining
  - Evaluation of *in vivo* antitumor efficacy
  - Evaluation of *in vivo* safety
- QUANTIFICATION AND STATISTICAL ANALYSIS

SUPPLEMENTAL INFORMATION

Supplemental information can be found online at https://doi.org/10.1016/j.isci.2024.110029.

ACKNOWLEDGMENTS

This work was supported by the National Key Research and Development Program of China (grant number: 2022YFC2408000), National Natural Science Foundation of China for Excellent Young Scientists (grant number: 82322039), NSFC projects (grant numbers: 82072063, 32001005, 32101136, and 82202306), Key Research and Development Program of Shaanxi Province (grant number: 2023-YBSF-132), Shaanxi Province Youth Science and Technology New Star (grant number: 2022KJXX-09), Natural Science Foundation of Shaanxi Province (grant numbers: 2020JQ610), the Medical-Engineering Cross Project of the First Affiliated Hospital of Xi'an Jiaotong University (grant number: QYJC02), and Science Foundation of Nanjing Chia Tai Tianqing Project (grant number: TQ202215).

AUTHOR CONTRIBUTIONS

The whole work was performed under the supervision of X.L., Y.L., and B.Y. X.L., Y.L., B.Y., and H.L. performed the experiment design. H.L. and Z.Y. performed this experiment. X.W., J.Y., and J.G. provided experimental and equipment support. C.L., H.F., and Y.L. provided technical assistance. All authors performed the data analysis and read the manuscript.

DECLARATION OF INTERESTS

The authors declare no competing interests.

Received: February 21, 2024
Revised: April 25, 2024
Accepted: May 16, 2024
Published: May 21, 2024

REFERENCES

1. Vogel, A., Meyer, T., Sapisochin, G., Salem, R., and Saborowski, A. (2022). Hepatocellular carcinoma. Lancet *400*, 1345–1362. https://doi.org/10.1016/s0140-6736(22)01200-4.
2. Siegel, R.L., Miller, K.D., Fuchs, H.E., and Jemal, A. (2021). Cancer Statistics, 2021. CA Cancer J. Clin. *71*, 7–33. https://doi.org/10.3322/caac.21654.
3. Llovet, J.M., Ricci, S., Mazzaferro, V., Hilgard, P., Gane, E., Blanc, J.F., de Oliveira, A.C., Santoro, A., Raoul, J.L., Forner, A., et al. (2008). Sorafenib in advanced hepatocellular carcinoma. N. Engl. J. Med. *359*, 378–390. https://doi.org/10.1056/NEJMoa0708857.
4. Llovet, J.M., Kelley, R.K., Villanueva, A., Singal, A.G., Pikarsky, E., Roayaie, S., Lencioni, R., Koike, K., Zucman-Rossi, J., and Finn, R.S. (2021). Hepatocellular carcinoma. Nat. Rev. Dis. Prim. *7*, 6. https://doi.org/10.1038/s41572-020-00240-3.
5. Yang, J.D., Hainaut, P., Gores, G.J., Amadou, A., Plymoth, A., and Roberts, L.R. (2019). A global view of hepatocellular carcinoma: trends, risk, prevention and management. Nat. Rev. Gastroenterol. Hepatol. *16*, 589–604. https://doi.org/10.1038/s41575-019-0186-y.
6. Llovet, J.M., Montal, R., Sia, D., and Finn, R.S. (2018). Molecular therapies and precision medicine for hepatocellular carcinoma. Nat. Rev. Clin. Oncol. *15*, 599–616. https://doi.org/10.1038/s41571-018-0073-4.
7. Cabral, L.K.D., Tiribelli, C., and Sukowati, C.H.C. (2020). Sorafenib Resistance in Hepatocellular Carcinoma: The Relevance of Genetic Heterogeneity. Cancers *12*, 1576. https://doi.org/10.3390/cancers12061576.
8. Cheng, A.-L., Kang, Y.-K., Chen, Z., Tsao, C.-J., Qin, S., Kim, J.S., Luo, R., Feng, J., Ye, S., Yang, T.-S., et al. (2009). Efficacy and safety of sorafenib in patients in the Asia-Pacific region with advanced hepatocellular carcinoma: a phase III randomised, double-blind, placebo-controlled trial. Lancet Oncol. *10*, 25–34. https://doi.org/10.1016/s1470-2045(08)70285-7.
9. Zhu, Y.J., Zheng, B., Wang, H.Y., and Chen, L. (2017). New knowledge of the mechanisms of sorafenib resistance in liver cancer. Acta Pharmacol. Sin. *38*, 614–622. https://doi.org/10.1038/aps.2017.5.
10. Bruix, J., Qin, S., Merle, P., Granito, A., Huang, Y.-H., Bodoky, G., Pracht, M., Yokosuka, O., Rosmorduc, O., Breder, V., et al. (2017). Regorafenib for patients with hepatocellular carcinoma who progressed on sorafenib treatment (RESORCE): a randomised, double-blind, placebo-controlled, phase 3 trial. Lancet *389*, 56–66. https://doi.org/10.1016/s0140-6736(16)32453-9.
11. Burotto, M., Chiou, V.L., Lee, J.M., and Kohn, E.C. (2014). The MAPK pathway across different malignancies: a new perspective. Cancer *120*, 3446–3456. https://doi.org/10.1002/cncr.28864.
12. Luangdilok, S., Box, C., Harrington, K., Rhŷs-Evans, P., and Eccles, S. (2011). MAPK and PI3K signalling differentially regulate angiogenic and lymphangiogenic cytokine secretion in squamous cell carcinoma of the head and neck. Eur. J. Cancer *47*, 520–529. https://doi.org/10.1016/j.ejca.2010.10.009.
13. Bernatchez, P.N., Allen, B.G., Gélinas, D.S., Guillemette, G., and Sirois, M.G. (2001). Regulation of VEGF-induced endothelial cell PAF synthesis: role of p42/44 MAPK, p38 MAPK and PI3K pathways. Br. J. Pharmacol. *134*, 1253–1262. https://doi.org/10.1038/sj.bjp.0704367.
14. Lei, Y., Chen, X., Mo, J.L., Lv, L.L., Kou, Z.W., and Sun, F.Y. (2023). Vascular endothelial growth factor promotes transdifferentiation of astrocytes into neurons via activation of the MAPK/Erk-Pax6 signal pathway. Glia *71*, 1648–1666. https://doi.org/10.1002/glia.24361.
15. Adya, R., Tan, B.K., Punn, A., Chen, J., and Randeva, H.S. (2008). Visfatin induces human endothelial VEGF and MMP-2/9 production via MAPK and PI3K/Akt signalling pathways: novel insights into visfatin-induced angiogenesis. Cardiovasc. Res. *78*, 356–365. https://doi.org/10.1093/cvr/cvm111.
16. Samatar, A.A., and Poulikakos, P.I. (2014). Targeting RAS-ERK signalling in cancer: promises and challenges. Nat. Rev. Drug Discov. *13*, 928–942. https://doi.org/10.1038/nrd4281.
17. Liu, F., Yang, X., Geng, M., and Huang, M. (2018). Targeting ERK, an Achilles' Heel of the MAPK pathway, in cancer therapy. Acta Pharm. Sin. B *8*, 552–562. https://doi.org/10.1016/j.apsb.2018.01.008.
18. Kun, E., Tsang, Y.T.M., Ng, C.W., Gershenson, D.M., and Wong, K.K. (2021). MEK inhibitor resistance mechanisms and recent developments in combination trials. Cancer Treat Rev. *92*, 102137. https://doi.org/10.1016/j.ctrv.2020.102137.
19. Lee, S., Rauch, J., and Kolch, W. (2020). Targeting MAPK Signaling in Cancer: Mechanisms of Drug Resistance and Sensitivity. Int. J. Mol. Sci. *21*, 1102. https://doi.org/10.3390/ijms21031102.
20. Liu, X.L., Yang, Y., Ng, C.T., Zhao, L.Y., Zhang, Y., Bay, B.H., Fan, H.M., and Ding, J. (2015). Magnetic vortex nanorings: a new class of hyperthermia agent for highly efficient in vivo regression of tumors. Adv. Mater. *27*, 1939–1944. https://doi.org/10.1002/adma.201405036.
21. Pan, J., Xu, Y., Wu, Q., Hu, P., and Shi, J. (2021). Mild Magnetic Hyperthermia-Activated Innate Immunity for Liver Cancer Therapy. J. Am. Chem. Soc. *143*, 8116–8128. https://doi.org/10.1021/jacs.1c02537.
22. Gu, N., Zhang, Z., and Li, Y. (2021). Adaptive iron-based magnetic nanomaterials of high performance for biomedical applications. Nano Res. *15*, 1–17. https://doi.org/10.1007/s12274-021-3546-1.
23. Liu, X., Zhang, Y., Guo, Y., Jiao, W., Gao, X., Lee, W.S.V., Wang, Y., Deng, X., He, Y., Jiao, J., et al. (2021). Electromagnetic Field-Programmed Magnetic Vortex Nanodelivery System for Efficacious Cancer Therapy. Adv. Sci. *8*, e2100950. https://doi.org/10.1002/advs.202100950.
24. Liu, X.L., Chen, S., Zhang, H., Zhou, J., Fan, H.M., and Liang, X.-J. (2019). Magnetic Nanomaterials for Advanced Regenerative Medicine: The Promise and Challenges. Adv. Mater. *31*, e1804922. https://doi.org/10.1002/adma.201804922.
25. Liu, X., Zhang, Y., Wang, Y., Zhu, W., Li, G., Ma, X., Zhang, Y., Chen, S., Tiwari, S., Shi, K., et al. (2020). Comprehensive understanding of magnetic hyperthermia for improving antitumor therapeutic efficacy. Theranostics *10*, 3793–3815. https://doi.org/10.7150/thno.40805.
26. Pinel, S., Thomas, N., Boura, C., and Barberi-Heyob, M. (2019). Approaches to physical stimulation of metallic nanoparticles for glioblastoma treatment. Adv. Drug Deliv. Rev. *138*, 344–357. https://doi.org/10.1016/j.addr.2018.10.013.
27. Clerc, P., Jeanjean, P., Hallali, N., Gougeon, M., Pipy, B., Carrey, J., Fourmy, D., and Gigoux, V. (2018). Targeted Magnetic Intra-Lysosomal Hyperthermia produces lysosomal reactive oxygen species and causes Caspase-1 dependent cell death. J. Control. Release *270*, 120–134. https://doi.org/10.1016/j.jconrel.2017.11.050.
28. Yan, B., Liu, C., Li, H., Wen, N., Jiao, W., Wang, S., Zhang, Y., Zhang, T., Zhang, H., Lv, Y., et al. (2023). Reversal of HMGA1-Mediated Immunosuppression Synergizes with

Immunogenic Magnetothermodynamic for Improved Hepatocellular Carcinoma Therapy. ACS Nano *17*, 9209–9223. https://doi.org/10.1021/acsnano.3c00004.

29. Yan, B., Liu, C., Wang, S., Li, H., Jiao, J., Lee, W.S.V., Zhang, S., Hou, Y., Hou, Y., Ma, X., et al. (2022). Magnetic hyperthermia induces effective and genuine immunogenic tumor cell death with respect to exogenous heating. J. Mater. Chem. B *10*, 5364–5374. https://doi.org/10.1039/d2tb01004f.
30. Liu, X., Yan, B., Li, Y., Ma, X., Jiao, W., Shi, K., Zhang, T., Chen, S., He, Y., Liang, X.J., and Fan, H. (2020). Graphene Oxide-Grafted Magnetic Nanorings Mediated Magnetothermodynamic Therapy Favoring Reactive Oxygen Species-Related Immune Response for Enhanced Antitumor Efficacy. ACS Nano *14*, 1936–1950. https://doi.org/10.1021/acsnano.9b08320.
31. Liu, X., Zheng, J., Sun, W., Zhao, X., Li, Y., Gong, N., Wang, Y., Ma, X., Zhang, T., Zhao, L.Y., et al. (2019). Ferrimagnetic Vortex Nanoring-Mediated Mild Magnetic Hyperthermia Imparts Potent Immunological Effect for Treating Cancer Metastasis. ACS Nano *13*, 8811–8825. https://doi.org/10.1021/acsnano.9b01979.
32. Zhao, Z., Zhang, D., Wu, F., Tu, J., Song, J., Xu, M., and Ji, J. (2021). Sophoridine suppresses lenvatinib-resistant hepatocellular carcinoma growth by inhibiting RAS/MEK/ERK axis via decreasing VEGFR2 expression. J. Cell Mol. Med. *25*, 549–560. https://doi.org/10.1111/jcmm.16108.
33. Zhang, G., He, J., Ye, X., Zhu, J., Hu, X., Shen, M., Ma, Y., Mao, Z., Song, H., and Chen, F. (2019). β-Thujaplicin induces autophagic cell death, apoptosis, and cell cycle arrest through ROS-mediated Akt and p38/ERK MAPK signaling in human hepatocellular carcinoma. Cell Death Dis. *10*, 255. https://doi.org/10.1038/s41419-019-1492-6.
34. Zhang, X., Zhang, P., An, L., Sun, N., Peng, L., Tang, W., Ma, D., and Chen, J. (2020). Miltirone induces cell death in hepatocellular carcinoma cell through GSDME-dependent pyroptosis. Acta Pharm. Sin. B *10*, 1397–1413. https://doi.org/10.1016/j.apsb.2020.06.015.
35. Su, X., Shen, Z., Yang, Q., Sui, F., Pu, J., Ma, J., Ma, S., Yao, D., Ji, M., and Hou, P. (2019). Vitamin C kills thyroid cancer cells through ROS-dependent inhibition of MAPK/ERK and PI3K/AKT pathways via distinct mechanisms. Theranostics *9*, 4461–4473. https://doi.org/10.7150/thno.35219.
36. Zhou, X., Wang, Y., Lee, W.Y.W., Or, P.M.Y., Wan, D.C.C., Kwan, Y.W., and Yeung, J.H.K. (2015). Miltirone Is a Dual Inhibitor of P-Glycoprotein and Cell Growth in Doxorubicin-Resistant HepG2 Cells. J. Nat. Prod. *78*, 2266–2275. https://doi.org/10.1021/acs.jnatprod.5b00516.
37. Wang, C., Jin, H., Gao, D., Lieftink, C., Evers, B., Jin, G., Xue, Z., Wang, L., Beijersbergen, R.L., Qin, W., and Bernards, R. (2018). Phospho-ERK is a biomarker of response to a synthetic lethal drug combination of sorafenib and MEK inhibition in liver cancer. J. Hepatol. *69*, 1057–1065. https://doi.org/10.1016/j.jhep.2018.07.004.
38. Rudalska, R., Dauch, D., Longerich, T., McJunkin, K., Wuestefeld, T., Kang, T.W., Hohmeyer, A., Pesic, M., Leibold, J., von Thun, A., et al. (2014). In vivo RNAi screening identifies a mechanism of sorafenib resistance in liver cancer. Nat. Med. *20*, 1138–1146. https://doi.org/10.1038/nm.3679.
39. Li, D., Wang, T., Sun, F.F., Feng, J.Q., Peng, J.J., Li, H., Wang, C., Wang, D., Liu, Y., Bai, Y.D., et al. (2021). MicroRNA-375 represses tumor angiogenesis and reverses resistance to sorafenib in hepatocarcinoma. Cancer Gene Ther. *28*, 126–140. https://doi.org/10.1038/s41417-020-0191-x.
40. Xu, J., Ji, L., Ruan, Y., Wan, Z., Lin, Z., Xia, S., Tao, L., Zheng, J., Cai, L., Wang, Y., et al. (2021). UBQLN1 mediates sorafenib resistance through regulating mitochondrial biogenesis and ROS homeostasis by targeting PGC1β in hepatocellular carcinoma. Signal Transduct. Targeted Ther. *6*, 190. https://doi.org/10.1038/s41392-021-00594-4.
41. Zhai, B., Hu, F., Jiang, X., Xu, J., Zhao, D., Liu, B., Pan, S., Dong, X., Tan, G., Wei, Z., et al. (2014). Inhibition of Akt reverses the acquired resistance to sorafenib by switching protective autophagy to autophagic cell death in hepatocellular carcinoma. Mol. Cancer Therapeut. *13*, 1589–1598. https://doi.org/10.1158/1535-7163.MCT-13-1043.
42. Xu, J., Ji, L., Liang, Y., Wan, Z., Zheng, W., Song, X., Gorshkov, K., Sun, Q., Lin, H., Zheng, X., et al. (2020). CircRNA-SORE mediates sorafenib resistance in hepatocellular carcinoma by stabilizing YBX1. Signal Transduct. Targeted Ther. *5*, 298. https://doi.org/10.1038/s41392-020-00375-5.

STAR★METHODS

KEY RESOURCES TABLE

REAGENT or RESOURCE	SOURCE	IDENTIFIER
Antibodies		
RAF1 Polyclonal antibody	Proteintech	Cat# 26863-1-AP, RRID: AB_2880660
MEK1/2 Polyclonal antibody	Proteintech	Cat# 11049-1-AP, RRID: AB_2140649
ERK1/2 polyclonal antibody	Proteintech	Cat# 16443-1-AP, RRID: AB_10603369
Phospho-ERK1/2 (Thr202/Tyr204) Polyclonal antibody	Proteintech	Cat# 28733-1-AP, RRID: AB_2881202
GAPDH Polyclonal antibody	Proteintech	Cat# 10494-1-AP, RRID: AB_2263076
HRP-conjugated Affinipure Goat Anti-Rabbit IgG(H + L)	Proteintech	Cat# SA00001-2, RRID: AB_2722564
Anti-MEK1 plus MEK2 (phospho-S221 + S222) antibody	Abcam	Cat# ab278723
Phospho-MEK1/2 (Ser221) antibody	Affinity	Cat# AF3385, RRID: AB_2834816
Chemicals, peptides, and recombinant proteins		
$FeCl_3 \cdot 6H_2O$	Sigma-Aldrich	Cat# 236489
$NH_4H_2PO_4$	Sigma-Aldrich	Cat# 216003
NaCl	Sigma-Aldrich	Cat# 793566
1-octadecene	Sigma-Aldrich	Cat# 74740
Oleic acid	Sigma-Aldrich	Cat# 01008
Dopamine hydrochloride	Thermo Fisher Scientific	Cat# A11136.14
Sorafenib	Selleck	Cat# S7397
PD98059	Selleck	Cat# S1177
LPS	Beyotime	Cat# S1732
RIPA Lysis Buffer	Beyotime	Cat# P0013B
Critical commercial assays		
CCK-8 Kit	Beyotime	Cat# C0038
crystal violet staining solution	Beyotime	Cat# C0121
Annexin V-FITC apoptosis detection kit	Beyotime	Cat# C1062
Reactive Oxygen Species Assay Kit	Beyotime	Cat# S0033
Enhanced BCA Protein Assay Kit	Beyotime	Cat# P0010
Hematoxylin-Eosin (HE) Stain Kit	Solarbio	Cat# G1120
Experimental models: Cell lines		
HuH-7	Procell Life Science & Technology Corporation	Cat# CL-0120
HuH-7/SR	This paper	N/A
AML-12	American Type Culture Collection	Cat# CRL-2254
Experimental models: Organisms/strains		
Mouse: BALB/c nude	Vital River Laboratory Animal Technology Corporation	Cat# 401
Software and algorithms		
GraphPad Prism 8.0.1	GraphPad	https://www.graphpad.com
Fiji	National Institutes of Health	https://fiji.sc
Origin 2021	Originlab	https://www.originlab.com
Image Pro Plus 6.0	Media Cybernetics	https://mediacy.com/image-pro
Flow Jo v.9.9.4	Flow Jo, LLC	https://www.flowjo.com

RESOURCE AVAILABILITY

Lead contact

Further information and requests for resources and reagents should be directed to and will be fulfilled by the lead contact, Xiaoli Liu (liuxiaoli0108@xjtu.edu.cn).

Materials availability

The FVIO are available on a reasonable request from the lead contact, Xiaoli Liu (liuxiaoli0108@xjtu.edu.cn).

Data and code availability

All data reported in this paper will be shared by the lead contact upon request.

This paper does not report original code.

Any additional information required to reanalyze the data reported in this paper is available from the lead contact upon request.

EXPERIMENTAL MODEL AND STUDY PARTICIPANT DETAILS

The human HCC cell line HuH-7 was purchased from Procell Life Science & Technology Co., Ltd. (Wuhan, Hubei, China). The mouse normal hepatocyte AML-12 cells were purchased from the American Type Culture Collection. HuH-7/SR cell lines were constructed by our group. AML-12, HuH-7 and HuH-7/SR cell lines were cultured in DMEM medium (Gibco, Carlsbad, CA) supplemented with 10% (v/v) heat-inactivated fetal bovine serum (FBS, Biological Industries, Kibbutz Beit-Haemek, Israel) and 100 U/mL penicillin-streptomycin solution (Hyclone Laboratories Inc., Logan UT, USA) in an incubator at 37°C, 5% CO_2. Additionally, HuH-7/SR cells were cultured with 2 μM sorafenib in the DMEM medium to maintain sorafenib resistance. Cells in a logarithmic growth phase were selected for experiments. For all experiments, cells were harvested using 0.25% EDTA trypsin (Gibco, Carlsbad, CA, USA). Four-week-old male BALB/c nude mice were obtained from Beijing Vital River Laboratory Animal Technology Co., Ltd. (Beijing, China). All animal experimental procedures were approved by the Animal Ethics Committee of Northwestern University, China.

METHOD DETAILS

Preparation of FVIO

Dopamine hydrochloride-modified FVIO nanorings were fabricated in three steps. Firstly, α-Fe_2O_3 nanorings were synthesized according to a previously reported method[20,28]: α-Fe_2O_3 nanorings were first developed via a hydrothermal method, and Fe_3O_4 powder was obtained after reduction in a tube furnace at 450°C for 2 h under 5% H_2/95% Ar.

Then, 30 mg of Fe_3O_4 powder was dispersed by sonication in a mixture of 0.4 mL oleic acid and 10 g 1-octadecene. The mixture was rapidly heated to 280°C under the protection of Ar and stirred continuously for 40 min. After cooling to room temperature, Fe_3O_4 nanoparticles in the oil phase were collected by centrifugation (8000 × *g*, 10 min), then washed three times and dispersed in 4 mL tetrahydrofuran.

Finally, 150 mg dopamine hydrochloride was dispersed by sonication in a mixture of 2 mL Fe_3O_4 solution and 10 mL tetrahydrofuran solution. The resulting mixture was reacted at 55°C for 5 h. The product was separated by centrifugation (8000 × *g*, 10 min) and washed three times with ultrapure water to obtain dopamine-modified FVIO.

Characterization of FVIO

A medium-frequency electromagnetic field instrument was employed as an induction heating system (M5, Xi'an SuperMag Nanobiotechnology Co., Ltd., China). The size and morphology of the FVIO were measured using a transmission electron microscope (Tecnai F30, FEI, USA) and a scanning electron microscope (SU 8010, Hitachi, Japan). The X-ray diffraction pattern was obtained using a D8 advanced diffractometer system (Bruker, Germany). Fourier transform infrared spectroscopy (FT-IR) spectra were recorded using a Tensor 27 spectrometer (Bruker, Germany). The Malvern Zetasizer (Zetasizer 2000, Malvern, UK) was used to determine the hydrodynamic size and zeta potential distribution of the FVIO nanorings. To ensure the quantity of FVIO was consistent for the subsequent experiments, the FVIO concentration was represented as Fe concentration in the samples and was determined using an inductively coupled plasma mass spectrometer (ICP-MS, Agilent, 7900, USA).

Measurement of SAR value

The magnetic heating efficiency of FVIO was evaluated by determining the SAR value. The Fe concentration of the FVIO was measured by ICP-MS. We chose different concentration (50 μg/mL, 100 μg/mL, 150 μg/mL) of FVIO to be exposed to an AMF of 360 kHz and 300 Oe for 10 min. The temperature profiles were monitored using an optical fiber thermocouple. The SAR value was determined using the following equation:

$$SAR = C\frac{\Delta T}{\Delta t}\frac{1}{m_{Fe}}$$

where C is the specific heat capacity of the medium (4.18 J/g °C), m_{Fe} is the mass concentration of Fe in the samples, and $\Delta T/\Delta t$ is the initial slope of the curve. If there are significant initial thermal losses or inhomogeneous temperature across the sample, such a procedure can result in unknown errors in the determination of $\Delta T/\Delta t$. Thus, in order to minimize the errors, $\Delta T/\Delta t$ is calculated as the maximum slope of the curve.

Induction of a sorafenib-resistant cell line

Sorafenib-resistant cell lines were induced by adding stepwise concentrations of sorafenib to the medium during repeated passages. The IC_{50} value of sorafenib in HuH-7 cells was measured, and HuH-7 cells were used as the parental cell line for developing the sorafenib-resistant cell line. Cells in a logarithmic growth phase were incubated with a starting concentration of 0.5 μM sorafenib for 24 h, and then the cells were cultured in drug-free medium for 48 h. Subsequently, this procedure was repeated for 9 months by changing the sorafenib concentration to 0.5, 1, 2, 5, 10, 15, 20, 25 and 30 μM. Finally, the IC_{50} value of sorafenib was determined using a CCK-8 kit (Beyotime, Shanghai, China). After resistance was established, HuH-7/SR cells were cultured with 2 μM sorafenib in the DMEM medium to maintain sorafenib resistance.

Half maximal inhibitory concentration assay

HuH-7 or HuH-7/SR cells were added to 96-well plates (1×10^4 cells per well) and cultured with various concentrations of sorafenib (0, 0.5, 1, 2, 4, 10, 20, 40, 100, 200 and 400 μM) for 48 h. Then, the cell viability was measured using a CCK-8 kit at 450 nm on a microplate reader (Thermo Fisher Scientific, Wilmington, DE, USA). Non-linear curve fitting and IC_{50} value calculation were performed using GraphPad Prism 8.0 software (San Diego, CA, USA).

MH treatment and water bath heating of HuH-7/SR cells

FVIO were dissolved in concentrated nitric acid, the suspension was filtered through a 0.22 μm filter membrane, and the Fe concentration was determined using ICP-MS. HuH-7/SR cells were cultured in 35 mm cell culture dishes, the cells were co-incubated with various concentrations of FVIO for 24 h. Then, the existing medium was discarded, the cells were washed 3 times with PBS and fresh medium was added. The cell culture dish was sealed with sealing film (Parafilm, PM-996, USA), and then placed in a water bath at 43°C for 10 min or exposed to AMF (300 Oe, 360 kHz) for 10 min. The cells were then placed in an incubator at 37°C in 5% CO_2 for subsequent experiments.

Cellular uptake assay

A total of 1×10^5 HuH-7/SR cells were cultured in 6-well plates for 24 h. FVIO suspensions with designated Fe concentrations replaced the medium. After designated incubation times (0, 2, 4, 8, 16, 24 and 32 h), HuH-7/SR cells were washed three times with 1× PBS to remove redundant FVIO suspension. Cells were immersed in concentrated nitric acid (MOS). After 1 h incubation under gentle shaking, ICP-MS was used to analyze the Fe concentration.

In vitro cell cytotoxicity

The cell cytotoxicity was assayed using a CCK-8 kit (Beyotime) according to the manufacturer's protocol. Briefly, the cell suspension (100 μL) was inoculated into 96-well plates (1×10^4 cells per well), and then cultured in an incubator at 37°C in 5% CO_2 for 24 h. The supernatant was discarded, and FVIO suspension at various concentrations (0, 10, 20, 30, 40, 50, 75 and 100 μg/mL) was added to each well and then incubated for 24 h. Cell suspensions that were subjected to MH treatment were added to 96-well plates (100 μL per well), then incubated for 4 h. The supernatant was discarded and 20 μL CCK-8 reagent was added to each well and incubated for 1 h. The OD values of each well at 450 nm were detected using a microplate reader.

Colony formation assay and cell growth curve

A total of 5×10^5 HuH-7/SR cells were seeded in 35 mm cell culture dishes and placed in an incubator for 24 h, then cells were treated with DMEM, sorafenib, MH or MH plus sorafenib, respectively. The cells were harvested using 0.25% trypsin and reseeded in 35 mm cell culture dishes and placed in an incubator for 24 h. Then cells were harvested using 0.25% trypsin and resuspended in fresh medium before use in subsequent experiments.

To determine colony formation, HuH-7/SR cells were added to a 6-well plate (500 cells/well) and cultured at 37°C in 5% CO_2. The medium was refreshed every three days, cells were allowed to culture for 15 days when visible colonies appeared. The medium was discarded and cell colonies were fixed with 4% paraformaldehyde for 10 min, then stained with crystal violet staining solution (Beyotime) for 10 min at room temperature, and imaged.

To determine cell growth curves, 1×10^4 HuH-7/SR cells/well were inoculated into 96-well plates and then placed in an incubator at 37°C in 5% CO_2 for 12 h. The OD values/well at 450 nm were tested by the CCK-8 on 0 h, 24 h, 48 h, 72 h or 96 h, respectively. Then, the cell growth curve was plotted by GraphPad 8.0 software using the OD values and culture time.

Cell apoptosis assay

A total of 5×10^5 HuH-7/SR cells were seeded in 35 mm cell dishes. The cells were collected after treatment with DMEM, sorafenib, MH, or MH plus sorafenib, respectively, and the level of apoptosis was assayed using an Annexin V-FITC apoptosis detection kit (Beyotime) according to the manufacturer's protocol. Briefly, the cells were washed with ice-cold PBS two times. Then, the cells were centrifuged at 1000 × *g* for 5 min

and resuspended in 195 μL 1 × binding buffer, and 5 μL Annexin V-FITC and 10 μL PI were added to the cells for 30 min at room temperature. A total of 1 × 10^4 cells were analyzed using a CyFlow Space cytometer (Sysmex Corporation, Kobe, Hyogo, Japan). The flow cytometry data were analyzed with FlowJo software.

Analysis of *in vitro* ROS generation

HuH-7/SR cells were pre-seeded in 35 mm glass-bottomed cell culture dishes at a density of 1 × 10^5 cells/dish. The cells were treated with DMEM, FVIO (75 μg/mL), or NAC (3 mM) plus FVIO (75 μg/mL) for 24 h. Cells were then washed 3 times with PBS, and incubated with 1 mL serum-free DMEM and 1 μL DCFH-DA (Beyotime) in the dark at 37°C for 20 min. The cells were then washed 3 times with serum-free medium and exposed to AMF (300 Oe, 360 kHz) for 10 min. The cells were immediately examined under a laser scanning confocal microscope (Nikon A1 Rsi, Nikon, Tokyo, Japan at 488 nm excitation and 525 nm emission).

Western blotting assay

After the corresponding treatments, the total protein was extracted from cells using 100 μL RIPA lysis solution (Beyotime) and the supernatant was collected by centrifugation at 12000*g* for 10 min at 4°C. The protein concentration was assayed using a BCA protein concentration kit (Beyotime). The protein was mixed with 6 × SDS loading buffer (Beyotime) at a ratio of 6:1 and boiled at 95°C–100°C for 10 min. Then 40 μg protein was separated by 10% sodium dodecyl sulphate-polyacrylamide gel electrophoresis (SDS-PAGE) and transferred to polyvinylidene fluoride (PVDF) membranes (Biosharp, Hefei, China). Non-specific binding antigenic sites on the PVDF membranes were blocked using 5% skimmed milk for 4 h. The immune blots were incubated overnight at 4°C with antibodies (RAF, MEK, ERK, *p*-ERK, Proteintech, 1:1000; *p*-MEK, Abcam, 1:2000; GAPDH, Proteintech, 1:5000) and then incubated with the corresponding secondary antibody (Proteintech, 1:10000) for 2 h at room temperature. The immune blots were washed with Tris-buffered saline Tween (TBST) solution three times. The results of the experiments were assayed using a western blot imaging system (Tanon, Shanghai, China). ImageJ software was used for quantification and analysis.

Development of a sorafenib-resistant HCC mouse model

A sorafenib-resistant HCC model was established using a slight modification to a previous study protocol.[41] Four-week-old male BALB/c nude mice were obtained from Beijing Vital River Laboratory Animal Technology Co., Ltd. (Beijing, China). All animal experimental procedures were approved by the Animal Ethics Committee of Northwestern University, China. To establish the model, 1×10^7 HuH-7/SR cells or 1×10^7 HuH-7 cells were injected subcutaneously into the right flank of BABL/c nude mice (n = 2), and mice in the HuH-7/SR group were given sorafenib 15 mg/kg daily for 6 weeks before all mice were sacrificed. Immunohistochemistry was performed on tumor samples from the mice.

Immunohistochemistry analysis and hematoxylin-eosin staining

Tissue samples were collected following *in vivo* experiments and fixed in 4% paraformaldehyde. The tumor tissues were embedded in paraffin, dewaxed and rehydrated, and 4-mm sections were subjected to antigen repair and nonspecific protein blocking using 5% BSA at room temperature for 30 min. The glass slides were incubated with anti-*p*-ERK (Proteintech, 1:100) and anti-*p*-MEK (Affinity, 1:100) antibodies overnight at 4°C followed by counterstaining according to standard methods. Conjugated secondary antibodies and diaminobenzidine were applied to visualize the protein, and samples were analyzed under an optical microscope (Nikon Eclipse E100). Finally, the integrated optical density (IOD) and area of the images were measured using Image Pro Plus 6.0 software (Media Cybernetics Inc., San Diego, CA, USA), and the mean density (IOD/area) was calculated to account for protein expression differences. The mouse tissues including the brain, heart, liver, spleen, lung, kidney and tumor were harvested for hematoxylin-eosin staining using a kit (Solarbio, Beijing, China) according to the manufacturer's protocol. Then, the results were observed using a microscope.

Evaluation of *in vivo* antitumor efficacy

First-generation sorafenib-resistant xenografts (n = 10) were developed according to previous methods. Then, all mice were sacrificed and tumor tissues were collected. Then, the tumor tissues were disaggregated into 1–2 mm^3 tissue samples, and inoculated into BALB/c nude mice to generate a sorafenib-resistant HCC tumor model. When tumor volumes reached approximately 100 mm^3, the tumor-bearing mice were randomized into 6 groups (n = 5 for each group), namely (1) control, (2) sorafenib, (3) FVIO-mediated MH, (4) FVIO-mediated MH plus PD98059, (5) FVIO-mediated MH plus sorafenib and (6) FVIO-mediated MH plus sorafenib plus PD98059. The mice were intratumorally injected with FVIO (3 mg Fe/cm^3) on day 1, and subjected to an AMF for 10 min (300 Oe, 360 kHz) on days 1, 3, and 5. PD98059 (2 mg/kg) was then intravenously injected on alternate days (on days 2, 4, and 6). Sorafenib (30 mg/kg) was administered to mice by oral gavage once every day. Tumor volume was measured with a caliper and calculated using the formula tumor volume = (length × $width^2$)/2. At the end of the experiment, all mice were sacrificed, and the tumor weights were recorded.

Evaluation of *in vivo* safety

Six-week-old SD rats randomly divided into two group (n = 3), received 200 μL of saline or saline containing FVIO (5.0 mg/kg Fe) intravenously. Serum sample were collected after injection on days 1 and 14. Parameters for determining liver function (ALT: alanine aminotransferase, AST: aspartate aminotransferase) and kidney function (BUN: blood urea nitrogen and CREA: creatinine) were measured using a Hitachi 7100 blood

biochemistry automatic analyzer 7100 (Hitachi Corp.). After 14 days of FVIO injection, all rats were euthanized. The heart, liver, spleen, lung, kidney and brain were collected after 14 days for H&E staining. Then, the results were observed using a microscope.

QUANTIFICATION AND STATISTICAL ANALYSIS

Statistical analyses were performed using GraphPad 8.0 software and Origin 2021. All data are expressed as the mean ± standard deviation (SD). The Student's t test and ANOVA were used to determine significant differences between test groups. $p < 0.05$ was regarded as indicating a significant difference. The Figures are annotated as follows: ns, no significant difference; *$p < 0.05$; **$p < 0.01$; ***$p < 0.001$; or ****$p < 0.0001$. See Table S1.